COMMUNICATION

Near-Infrared Fluorescent Molecular Probe for Sensitive Imaging of Keloids

Qingqing Miao[+], David Yeo[+], Christian Wiraja, Jianjian Zhang, Xiaoyu Ning, Chenjie Xu*, and Kanyi Pu*

Abstract: Early detection of skin diseases is imperative for their effective treatment. However, fluorescence molecular probes that allows this are rare. We herein report the first activatable near-infrared (NIR) fluorescent molecular probe for sensitive imaging of keloid cells, skin cells from abnormal scar fibrous lesions. As keloid cells have high expression levels of fibroblast activation protein-alpha (FAPα), the probe (FNP1) is designed to have a caged NIR dye and a FAPα-cleavable peptide substrate linked by a self-immolative segment. FNP1 can quickly and specifically turn on its fluorescence at 710 nm by 45-fold in the presence of FAPα, allowing it to effectively recognize keloid cells from normal skin cells. Integration of FNP1 with a simple microneedle-assisted topical application enables sensitive detection of keloid cells in metabolically-active human skin tissue with a theoretical limit of detection down to 20,000 cells. Thus, our probe holds great promise for early diagnosis of keloid scars.

Detection of skin diseases at early stage is critical to their timely treatment.[1] As fibrous scar lesions, keloids overgrow their wound boundaries due to over-exuberant healing following skin injury,[2] which causes limited joint mobility, psychological distress as well as significant pain and itch to those afflicted.[3] Current keloid management strategies including injection of steroids and anti-proliferative drugs, surgical excision and radiotherapy are often performed after visual assessment in clinics,[4] which have limited efficacy and even a high risk of keloid recurrence.[5] Such difficulty in keloid treatment necessitates the development of specific and sensitive diagnostic tools for keloids detection.

In addition to visual assessment, diffuse reflectance spectroscopy has been used to distinguish collagen alignment in keloids from that in healthy skin morphology.[6] However, because it simply relies on the intrinsic signals from clusters of endogenous biomolecules, this method is insensitive and only limited to imaging mature keloids.[6] By contrast, fluorescent molecular probes that change their signal in response to biomarkers have high signal-to-background ratio and thus are generally sensitive enough to detect diseases at relatively early stages.[7-10] However, to the best of our knowledge, such molecular probes have not been developed for keloids diagnosis.

In this study, we report the design and syntheses of near-infrared (NIR) fluorescence activatable molecular probes for specific detection of keloid-derived fibroblasts (KF). These probes can turn-on its NIR fluorescence in the presence of fibroblast activation protein-alpha (FAPα), which is overexpressed in activated keloid fibroblasts relative to normal fibroblasts.[11] As a type II transmembrane serine protease, FAPα plays a critical role in overgrowing the wound borders of keloids because it facilitates degradation of extracellular matrix (ECM) components such as gelatin and type I collagen,[12] which correlates with the "invasiveness" of keloids.

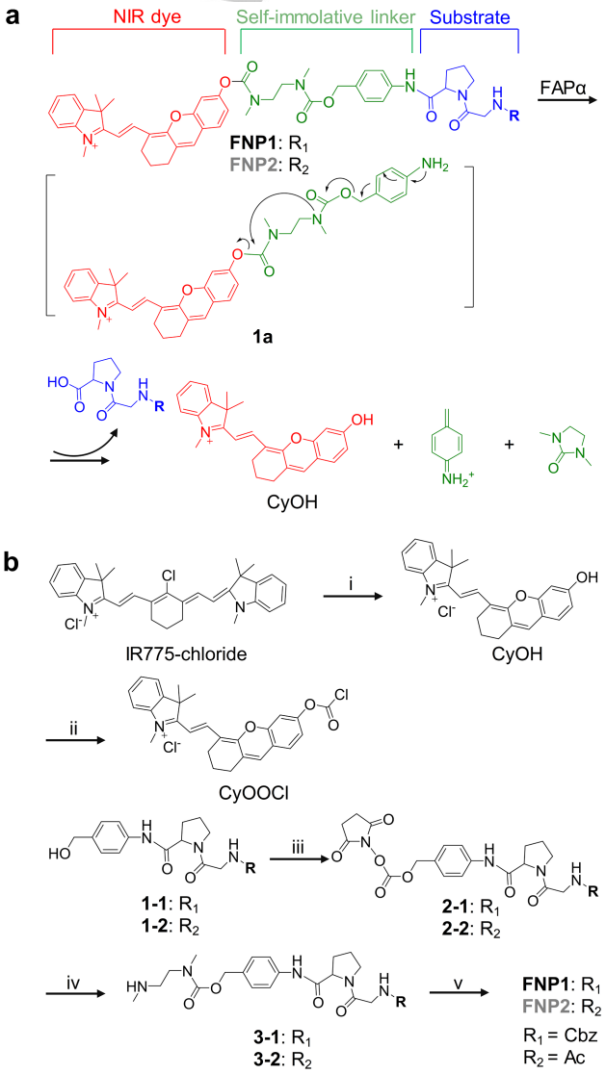

Scheme 1. (a) Design and mechanism of FNP1 or FNP2 for FAPα imaging. (b) Syntheses of FNP1 and FNP2. Reagents and conditions: (i) resorcinol, K_2CO_3, ACN, 50 °C, 6 h; (ii) triphosgene, anhydrous DCM, 25 °C, 0.5 h; (iii) N, N'-disuccinimidyl carbonate, DIPEA, anhydrous ACN, 25 °C,

[*] Dr. Q. Miao,[+] Dr. D. Yeo,[+] Dr. C. Wiraja, Dr. J. Zhang, X. Ning, Prof. C. Xu, Prof. K. Pu.
School of Chemical and Biomedical Engineering
Nanyang Technological University
Singapore, 637457 (Singapore)
E-mail: cjxu@ntu.edu.sg
kypu@ntu.edu.sg
[+] These authors contributed equally to this work

Supporting information and the ORCID identification number(s) for the author(s) of this article can be found under: https://doi.org/10.1002/anie.2017XXXXX

overnight. (iv) N,N'-dimethylethylenediamine, DIPEA, anhydrous THF, 25 °C, 8 h; (v) CyOOCl, K_2CO_3, anhydrous DCM, 25 °C, 5 h.

To achieve the specific and sensitive detection of FAPα, FAPα-activatable probes (FNP1 or FNP2) are designed by conjugating the peptide substrate, carbobenzyloxy-Gly-Pro-OH (Cbz-Gly-Pro) or acetyl-Gly-Pro-OH (Ac-Gly-Pro), with a NIR hemicyanine dye (CyOH)[13-15] through a carbamate-based self-immolative linker (**Scheme 1a**). Both probes are initially nonfluorescent because CyOH is in a "caged" state with diminished electron-donating ability of the oxygen atom. In the presence of FAPα, cleavage of the amide linkage between the peptide substrate and the self-immolative linker occurs to form the intermediate aniline **1a**, followed by 1,6-elimination and subsequently spontaneous cyclization of N, N'-dimethylethylenediamine, eventually leading to the free CyOH dye ("uncaged" state) with enhanced electron-donating ability from the oxygen atom (**Scheme 1**). Thus, the probes are able to turn on NIR fluorescence in response to FAPα. Note that only few FAPα-specific probes have been reported before, which rely on charge-transfer based quenching mechanism and have not been used for detection of keloids.[16-17]

Scheme 1 presents the synthetic route of the FAP probes. Firstly, the NIR moiety (CyOH) was obtained by reacting IR775-chloride with resorcinol via a retro-Knoevenagel reaction, followed by reacting with triphosgene to afford active chloroformate CyOOCl directly for the following reaction. Then, the *p*-aminobenzyl alcohol coupled peptide sequence (**1-1** or **1-2**) was conjugated with N, N'-disuccinimidyl carbonate to form N-hydroxysuccinimide carbonate (**2-1** or **2-2**), which was further treated with N, N'-dimethylethylenediamine to afford compound **3-1** or **3-2**. They were respectively reacted with active chloroformate CyOOCl to obtain FNP1 and FNP2.

To validate FAPα-induced cleavage as illustrated in **Scheme 1** and compare kinetics between FNP1 and FNP2 towards FAPα, absorption, fluorescence spectra and high performance liquid chromatography (HPLC) characterization were used to monitor the change of the probes from "caged" to "uncaged" state in both qualitative and quantitative ways (**Figure 1**a-e). Both FNP1 and FNP2 had the absorption maximum at 590 nm and were initially nonfluorescent. Upon treatment with FAPα (9.0×10^{-4} U mL^{-1}) for 25 min, FNP1 showed obvious decrease in the absorption peak at 590 nm with the emergence of a new peak at 682 nm assigned to the released free CyOH (**Figure 1**a&**Figure S1**a, Supporting Information). In comparison, FNP2 had subtle change in its absorption even after incubation with FAPα for 120 min (**Figure 1**a&**Figure S1**c, Supporting Information). The ratiometric absorption signal A_{682}/A_{590} (the ratio of the absorption intensity at 682 to that at 590 nm) was quantified as a function of incubation time at different concentrations of FAPα (**Figure S1**b). FNP1 showed increased A_{682}/A_{590} with increased incubation time and reached its plateau at 25 min, indicating the complete conversion of FNP1 into free CyOH. At this time point, FNP1 showed 45-fold enhancement in the fluorescence intensity at 710 nm, which was only 10-fold for FNP2. (**Figure 1**b). HPLC and electrospray ionization-mass spectrometry analyses further demonstrated that FNP1 (HPLC retention time, T_R = 24.8 min) was totally converted into free CyOH (T_R = 21.9 min) after 25 min incubation with FAPα; in contrast, FNP2 (T_R = 17.9 min) had only 14 and 33 % conversion after FAPα treatment for 25 and 120 min, respectively (**Figure 1**c, d, **Figure S1**d &**Figure S2**, Supporting Information).

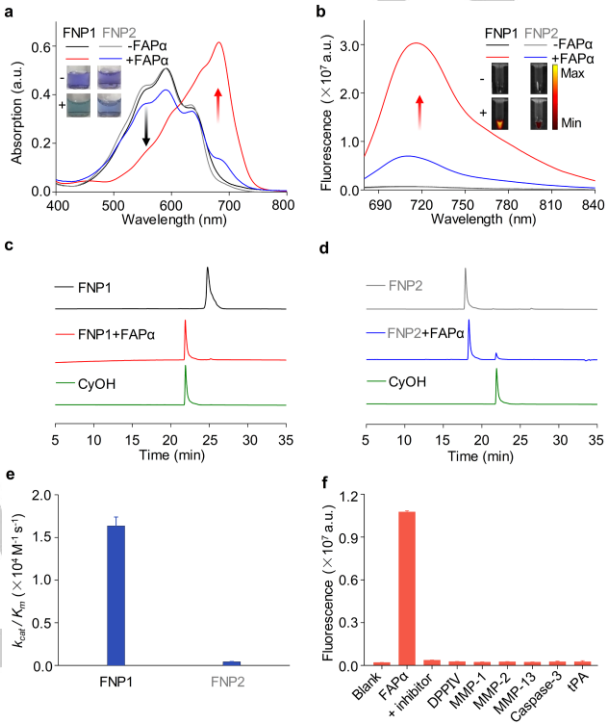

Figure 1. UV-Vis absorption spectra **(a)** and fluorescence **(b)** of FNP1 or FNP2 (10 μM) in the absence or presence of FAPα (9.0×10^{-4} U mL^{-1}) for 25 min at 37 ºC in HEPES buffer (50 mM, pH = 7.4) containing BSA (1 mg/mL) and glycerol (5%). Excitation: 660 nm. Inset: white light (**a**) and fluorescence (**b**) images of FNP1 (left panel) or FNP2 (right panel) (10 μM) in the absence or presence of FAPα (9.0×10^{-4} U mL^{-1}) for 25 min at 37 ºC in HEPES buffer (50 mM, pH = 7.4) containing 1mg/mL BSA and 5% glycerol. The fluorescence images were acquired at 720 nm upon excitation at 640 nm. HPLC traces of the incubation mixture of FNP1 **(c)** or FNP2 **(d)** in the absence (upper panel) or presence (middle panel) of FAP (9.0×10^{-4} U mL^{-1}), and HPLC traces of CyOH in water (lower panel). Wavelength: 600 nm. **(e)** Kinetics studies of FNP1 and FNP2 towards FAPα. **(f)** Fluorescence intensities of FNP1 (5.5 μM) at 710 nm after incubation with indicated enzymes for 30 min at 37 ºC. Excitation: 660 nm. The error bars represent the standard deviation from three separate measurements.

To quantitatively study the probe sensitivity, the enzymatic Michaelis-Menten constants (K_m) of FAPα towards FNP1 and FNP2 were calculated to be 46 and 185 μM, respectively (**Figure S3**, Supporting Information). This confirmed that the binding affinity of FNP1 to FAPα was 4.0-fold higher as compared with that of FNP2. Additionally, the catalytic rate constants (k_{cat}) of FAPα towards FNP1 and FNP2 were 0.755 and 0.0793 s^{-1}, respectively. Therefore, the catalytic efficiencies (k_{cat}/K_m) of FAPα towards FNP1 was calculated to be $1.64 \times 10^4 \pm 1.04 \times 10^3$ M^{-1} s^{-1}, 38.1-fold higher than that of FNP2 (**Figure 1**e). Thus, FNP1 was selected for detection of FAPα for the following studies. To determine its specificity, FNP1 activation was tested against FAPα in the presence of its inhibitor Val-boroPro (talabostat)[18] or

other enzymes relevant to skin diseases including dipeptidyl peptidase IV (DPPIV), matrix metalloproteinase (MMP)-1, MMP-2, MMP-13, caspase-3 and tissue plasminogen activator (tPA).[19] As shown in **Figure 1**f &**Figure** S4 in Supporting Information, the fluorescence intensity of FNP1 barely increases when FAPα was treated with inhibitor talabostat or in the presence of other enzymes, further validating FAPα induced FNP1 activation and confirming its high selectivity towards FAPα.

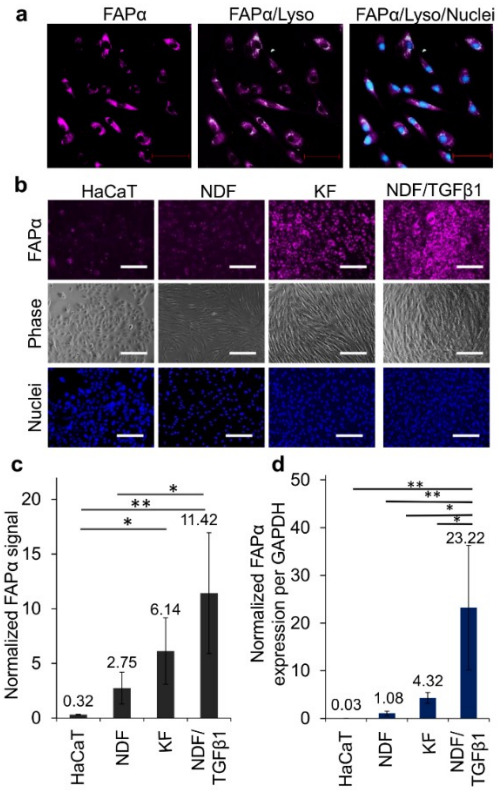

Figure 2. FNP1 probe in cell culture. **(a)** Fluorescence microscopy of KF cells after treatment with FNP1 (5 μM, purple) for 1 h and stained with nucleus indicator (Hoechst 33342, blue) for 30 min and lysosome indicator (LysoTracker®, white) for 30 min. Scale bar: 20 μm. **(b)** Fluorescence microscopy of HaCaT, NDF, KF and NDF cells stimulated with TGF-β1 (10 ng mL^{-1}) after treatment with FNP1 (5 μM, purple) for 1 h and stained with nucleus indicator (Hoechst 33342, blue) for 30 min. Scale bar: 100 μm. **(c)** Quantification of fluorescence intensities of the cells (HaCaT, NDF, KF, NDF+TGF-β1) after incubation with FNP1 in **Figure 2**b using multiplate reader. The fluorescence intensities of FNP1 were normalized by total cell nuclei signal (NucBlue®). **(d)** Relative gene expression of FAPα in HaCaT, NDF, KF, NDF+TGF-β1 normalized by GAPDH and NDF expression levels using qRT-PCR. The error bars represent the standard deviation from three separate measurements. *:$p < 0.05$, **:$p < 0.01$.

With its high sensitivity and fast kinetics, FNP1 was then applied to detect KF cells in culture along with the control skin cells including immortalized keratinocytes (HaCaT, epidermis origin) and normal dermal fibroblasts (NDF, dermis origin). After a short incubation period (1 h), strong NIR fluorescence was detected for KF (**Figure 2**a). Co-staining studies confirmed that FNP1 was mainly localized in the cytoplasm, including the cell lysosome. In contrast, weak fluorescence was observed in other cells including HaCaT and NDF (**Figure 2**b). Fluorescence quantification further revealed that the NIR fluorescence of FNP1 in KF cells was 19.2 and 2.23-fold higher than that in HaCaT and NDF, respectively (**Figure 2**c). Moreover, NDF cells were stimulated using transforming growth factor (TGF)-β1, well known to increase the expression levels of FAPα.[20] As shown in **Figures 2**b&**2**c, the NIR fluorescence of FNP1 in NDF cells was enhanced by 4.15-fold after TGF-β1 stimulation, confirming that the NIR signal of FNP1 was indeed correlated with the expression level of FAPα. To further validate this corrleation, reverse transcription-quantitative polymerase chain reaction (RT-qPCR) was conducted to quantify the gene expression of FAPα for all these cells ((**Figure 2**d)). The expression values of HaCaT, KF, NDF+TGF-β1 were 0.03, 4.32 and 23.2-fold relative to NDF's expression, respectively. Such an expression trend obtained from gene expression analysis was consistent with that for the fluorescent signals. Thus, these data proved that FNP1 could be specifically activated by FAPα, allowing for distinguishing KF cells from other normal skin cells (i.e. NDF, HaCaT).

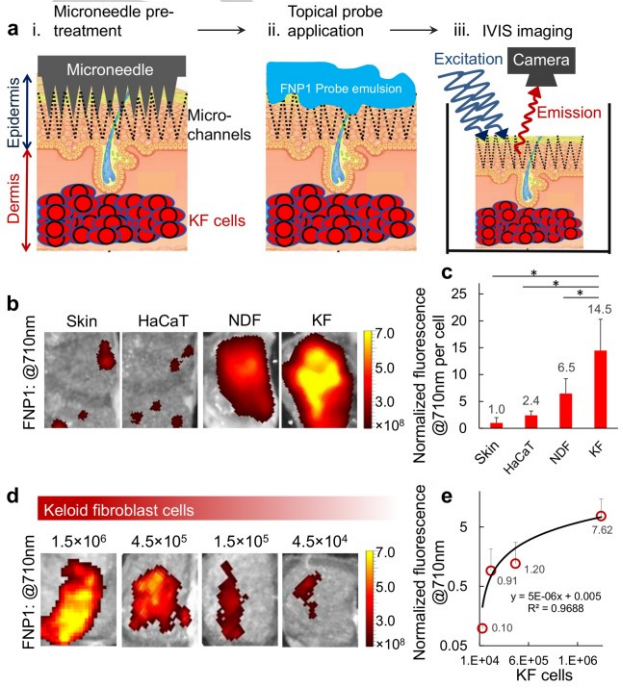

Figure 3. (a) Schematic illustration of microneedle-assisted penetration of FNP1 for FAPα imaging in keloid disease models. (i) Skin tissue pre-treated with microneedles to generate micro-channels (5 min, 16.7 kPa pressure), (ii) micro-channels facilitate FNP1 penetration, (iii) fluorescence imaging. **(b)** Representative fluorescence imaging of unmodified skin, skin implanted with HaCaT, NDF or KF cells after treatment with FNP1 (20 μL, 250 μM) for 6 h. **(c)** Quantification of fluorescence intensities of the skins from **Figure 3**b. The fluorescence intensities derived from FNP1 were normalized by total cell number (@570nm). **(d)** Representative fluorescence imaging of skin implanted with different amounts of KF cells ($1.5×10^6$, $4.5×10^5$, $1.5×10^5$ and $4.5×10^4$) after treatment with FNP1 (20 μL, 250 μM) for 6 h. **(e)** Quantification of fluorescence intensities of the skins in **Figure 3**d. The fluorescence intensities (@710nm) derived from FNP1 were normalized by background fluorescence. The error bars represent the standard deviation from three separate measurements. *: $p<0.05$.

Ability of FNP1 to detect KF cells was subsequently evaluated in live, metabolically-active human skin tissue models

containing diseased KF cells as a proof-of-concept. To successfully detect the implanted KF cells, FNP1 was mixed with Aquaphor® ointment to form an emulsion to help it cross the uppermost skin epidermal barrier to interact with dermis-residing KF cells for topical application. Initial trials using skin stripped of the epidermis (uppermost skin layer), showed that the probe readily diffused throughout the skin dermis, and detected KF cells within tissue at the depth of 1.4 mm at least (**Figure S5**, Supporting Information). However, when whole-skin models with intact epidermis barrier was used, the probe signal was mainly observed on the skin surface with negligible signal in the skin dermis (**Figure S5**, Supporting Information). These data showed that FNP1 was likely to be trapped in the uppermost skin layer, failing to cross the epidermis.

To facilitate the transdermal penetration of the hydrophilic probe, microneedles were employed to create microchannels (**Figure 3**a). Microneedle device (700~900 μm in height per needle) is enough to insert into skin at early stage of scar formation. The microneedles were weighted down to deform skin at 18-fold pressure magnitude below that required to break skin (i.e. 300 kPa).[21] After 5 min, the microneedles were removed and FNP1 was topically applied to the skin surface (**Figure 3**a) and incubated for 6 h before imaging. As shown in **Figures 3**b&**3**c, the NIR fluorescence of FNP1 from KF-implanted skin was 14.5, 6.5, and 2.4-fold higher than unmodified skin, HaCaT-implanted and NDF-implanted skin, respectively. The specificity of FNP1 to KF over NDF cells was further validated from skin tissue histology (**Figure S6**a, Supporting Information) throughout the entire skin tissue depth (1.2 mm) (**Figure S6**b, Supporting Information). These data demonstrated that the microneedle-assisted topical application of FNP1 allowed it to cross the epidermis layer to the dermis-residing cells for selective detection of KF cells.

To evaluate the sensitivity of FNP1 for detection of KF cells in human skin models, skins implanted with different amounts of KF cells (1.5×10^6, 4.5×10^5, 1.5×10^5 and 4.5×10^4) were tested. As shown in **Figure 3**d, the NIR fluorescent signal of FNP1 was still detectable with the numbers as low as 4.5×10^4 cells. An exponential relationship was observed between the NIR fluorescent signal magnitude and the number of KF cells (**Figure 3**e). Its theoretical relationship suggested that FNP1 could potentially detect a minimum of 20,000 KF cells by assuming a minimum observable signal of ~0.1. This was ~50-fold lower than the estimated number of cells (~1,000,000) within a mature keloid scar of 1 cm radius (assuming a spherical shape and cell density of 2.3×10^5 cells mL^{-1}).[22] Therefore, FNP1 should have the potential to detect early signs of abnormal scarring before progression into mature keloid scars.

In summary, we have developed the NIR molecular probes that can be activated by FAPα to turn on its NIR fluorescence for imaging of keloid cells. Such probes comprise a NIR dye (CyOH) and a FAPα-clevable peptide connected by a self-immolative linker. The optimal probe (FNP1) showed 45-fold fluorescence enhancement at 710 nm. With fast activation kinetics and high selectivity towards FAPα, FNP1 can clearly distinguish KF cells from other normal skin cells. Microneedle-assisted topical application faciliates the transdermal penetration of FNP1, enabling detection of KF cells in metabolically-active human skin tissue with a theoretical limit of detection as low as 20,000 cells. Such a high sensitivity implies that FNP1 could be potentially applied for early detection of abnormal scarring before progression into keloid scars. In addition to explore the application for early detection, the high sensitivity and selectivity of FNP1 will facilitate the development of monitoring and evaluation approaches after systematic therapy of abnormal scarring or keloids that have intrinsically overexpressed FAPα as an index. To the best our knowledge, our study represents the first smart molecular probe for sensitive imaging of keloid cells. Further modificaiton of CyOH can be a way to enhance the transdermal penetration of the probe for simplified in vivo detection..

Experimental Section

See the Supporting Information for materials, instruments, synthetic procedures and supporting figures (Figure S1-S17) and tables (Table S1-S3).

Acknowledgements

K.P. thanks Nanyang Technological University (Start-Up grant: NTUSUG: M4081627.120) and Singapore Ministry of Education (Academic Research Fund Tier 1: RG133/15 M4011559 and Academic Research Fund Tier 2 MOE2016-T2-1-098) for the financial support. C. X. thanks LKCMedicine-SCBE collaborative grant (CG-05/16) and NTU-NU nanomedicine grant (M4081502) for the financial support.

Conflict of interest

The authors declare no conflict of interest.

Keywords: molecular probe• fibroblast activation protein-alpha • near-infrared fluorescence imaging • skin diseases

[1] A. Esteva, B. Kuprel, R. A. Novoa, J. Ko, S. M. Swetter, H. M. Blau, S. Thrun, *Nature* **2017**, *542*, 115-118.
[2] S. Aarabi, M. T. Longaker, G. C. Gurtner, *PLoS Med.* **2007**, *4*, e234.
[3] A. Bayat, D. A. McGrouther, M. W. J. Ferguson, *Brit. Med. J.* **2003**, *326*, 88-92.
[4] R. B. Ahuja, P. Chatterjee, *Burns* **2014**, *40*, 583-588.
[5] A. Al-Attar, S. Mess, J. M. Thomassen, C. L. Kauffman, S. P. Davison, *Plast. Reconstr. Surg.* **2006**, *117*, 286-300.
[6] C.-K. Hsu, S.-Y. Tzeng, C.-C. Yang, J. Y.-Y. Lee, L. L.-H. Huang, W.-R. Chen, M. Hughes, Y.-W. Chen, Y.-K. Liao, S.-H. Tseng, *Biomed. Opt. Express* **2015**, *6*, 390-404.
[7] J. F. Lovell, T. W. B. Liu, J. Chen, G. Zheng, *Chem. Rev.* **2010**, *110*, 2839-2857.
[8] Q. Miao, K. Pu, *Bioconjug. Chem.* **2016**, *27*, 2808-2823.
[9] G. Liang, H. Ren, J. Rao, *Nat. Chem.* **2010**, *2*, 54-60.
[10] J. Zhou, X. Du, B. Xu, *Angew. Chem. Int. Ed.* **2016**, *55*, 5770-5775; *Angew. Chem.* **2016**, *128*, 5864– 5869.
[11] J. Canady, S. Arndt, S. Karrer, A. K. Bosserhoff, *J. Invest. Dermatol.* **2013**, *133*, 647-657.
[12] Y. Huang, A. E. Simms, A. Mazur, S. Wang, N. R. León, B. Jones, N. Aziz, T. Kelly, *Clin. Exp. Metastasis* **2011**, *28*, 567-579.

[13] L. Yuan, W. Lin, S. Zhao, W. Gao, B. Chen, L. He, S. Zhu, *J. Am. Chem. Soc.* **2012**, *134*, 13510-13523.
[14] J. Zhang, C. Li, R. Zhang, F. Zhang, W. Liu, X. Liu, S. M. Lee, H. Zhang, *Chem. Commun.* **2016**, *52*, 2679-2682.
[15] Z. Luo, L. Feng, R. An, G. Duan, R. Yan, H. Shi, J. He, Z. Zhou, C. Ji, H.-Y. Chen, D. Ye, *Chem. Eur. J.* **2017**, *23*, 14778-14785.
[16] J. Li, K. Chen, H. Liu, K. Cheng, M. Yang, J. Zhang, J. D. Cheng, Y. Zhang, Z. Cheng, *Bioconjugate Chem.* **2012**, *23*, 1704-1711.
[17] T. Ji, Y. Zhao, J. Wang, X. Zheng, Y. Tian, G. Nie, *Small* **2013**, *9*, 2427-2431.
[18] K. Narra, S. R. Mullins, H.-O. Lee, B. Strzemkowski-Brun, K. Magalong, V. J. Christiansen, P. A. Mckee, B. Egleston, S. J. Cohen, L. M. Weiner, N. J. Meropol, J. D. Cheng, *Cancer Biol. Ther.* **2007**, *6*, 1691-1699.
[19] T.-L. Tuan, H. Wu, E. Y. Huang, S. S. N. Chong, W. Laug, D. Messadi, P. Kelly, A. Le, *Am. J. Pathol.* **2003**, *162*, 1579-1589.
[20] M. M. Koczorowska, S. Tholen, F. Bucher, L. Lutz, J. N. Kizhakkedathu, O. De Wever, U. F. Wellner, M. L. Biniossek, A. Stahl, S. Lassmann, O. Schilling, *Mol. Oncol.* **2016**, *10*, 40-58.
[21] G. S. Ashcroft, T. Greenwell-Wild, M. A. Horan, S. M. Wahl, M. W. J. Ferguson, *Am. J. Pathol.* **1999**, *155*, 1137-1146.
[22] V. Lee, G. Singh, J. P. Trasatti, C. Bjornsson, X. Xu, T. N. Tran, S.-S. Yoo, G. Dai, P. Karande, *Tissue Eng. Part C Methods* **2014**, *20*, 473-484.

Entry for the Table of Contents (Please choose one layout)

Layout 1:

COMMUNICATION

Topical Molecular NIR Keloid Probe: A highly sensitive NIR probe specific to FAPα was designed for minimally-invasive keloid scar diagnosis. Through topical application and skin imaging, low cell numbers (20,000 cells) can be attained for early-stage keloid diagnosis.

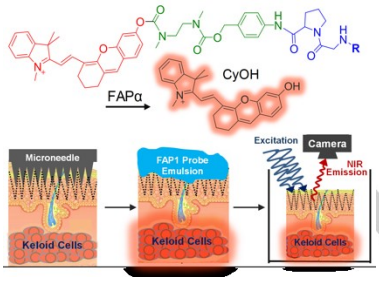

Qingqing Miao[+], David Yeo[+], Christian Wiraja, Xiaoyu Ning, Jianjian Zhang, Chenjie Xu, and Kanyi Pu**

Page XXXX – Page XXXX

Near-Infrared Fluorescent Molecular Probe for Sensitive Imaging of Keloids